J Electroceram (2017) 38:176–181
DOI 10.1007/s10832-016-0058-6

Microelectrodes for local conductivity and degradation measurements on Al stabilized $Li_7La_3Zr_2O_{12}$ garnets

Andreas Wachter-Welzl[1] · R. Wagner[2] · D. Rettenwander[3] · S. Taibl[1] · G. Amthauer[2] · J. Fleig[1]

Received: 26 August 2016 / Accepted: 14 November 2016 / Published online: 23 November 2016

Abstract The attractiveness of $Li_7La_3Zr_2O_{12}$ (LLZO) cubic based garnets lies in their high ionic conductivity and the combination of thermal and electrochemical stability. However, relations between composition and conductivity as well as degradation effects are still not completely understood. In this contribution we demonstrate the applicability of microelectrodes (Ø = 20–300 μm) for electrochemical impedance spectroscopy (EIS) studies on LLZO garnets. Microelectrodes allow to obtain local information on the ionic conductivity. A comparison between the overall performance of the sample (3.3×10^{-4} S cm^{-1}) and local measurements revealed differences in conductivity with a maximum of the locally measured values of 6.3×10^{-4} S cm^{-1} and a minimum of 2.6×10^{-4} S cm^{-1}. One reason behind these conductivity variations is most probably a compositional gradient in the sample. In addition, microelectrodes are very sensitive to conductivity changes near to the surface. This was used to investigate the effect of moisture in ambient air on the conductivity variations of LLZO. Substantial changes of the measured Li-ion transport resistance were found, particularly for smaller microelectrodes which probe sample volumes close to the surface.

✉ Andreas Wachter-Welzl
Andreas.Wachter-Welzl@tuwien.ac.at

[1] Institute for Chemical Technologies and Analytics, Vienna University of Technology, Getreidemarkt 9, BC – EG 164, 1060 Vienna, Austria

[2] Department of Chemistry and Physics of Materials, University of Salzburg, Hellbrunnerstrasse 34, Salzburg 5020, Austria

[3] Department of Materials Science and Engineering, Massachusetts Institute of Technology, 77 Massachusetts Avenue, Cambridge, MA 02139, USA

Keywords Li-ion batteries · Solid electrolyte · Impedance spectroscopy · Conductivity · Microelectrode · LLZO

1 Introduction

Storage and conversion of electrical energy is one of the major topics of current scientific activities and the search for optimized materials is key for technologies such as mobile devices, electric vehicles and load levelling. Li-ion batteries based on organic electrolytes are already widely used but suffer from several issues such as safety and stability problems as well as limitations in energy density. Therefore, solid materials came into the focus of electrolyte research. One promising class of ceramic ion conductors for future Li-ion battery systems is based on cubic $Li_7La_3Zr_2O_{12}$ (LLZO) and variants stabilized at room temperature by substitution of aliovalent ions [1–4]. Numerous doping elements were tested, including Al, Ga, Ta, Nb, Mo, Fe and LLZO garnets, and conductivities in the range of 10^{-4} – 10^{-3} S cm^{-1} have been achieved [5].

However, there is still substantial scatter of conductivity data in literature. For example, Al stabilized LLZO with very similar nominal composition of $Li_{7-3x}Al_xLa_3Zr_2O_{12}$ with x = 0.17–0.25, total conductivities in the range of 1.4–5.7×10^{-4} S cm^{-1} are reported [6–8]. This suggests that still unknown parameters, possibly associated with sintering, affect the conductivity. Among others, lithium evaporation may play a role and inhomogeneous samples may thus result. Moreover, degradation of the conductivity was found and may originate in near-surface regions due to interaction with the gas phase containing H_2O and CO_2 [9–14]. In principle microelectrodes enable the investigation of local conductivities in solid electrolytes and thus may help clarifying reasons behind the data scattering and the sample degradation [15–18]. Impedance spectroscopic studies on circular

microelectrodes with diameters of a few micrometres (≈ 10 μm) can reveal the bulk conductivity of a similarly sized region beneath and are also very sensitive to any higher or lower conductivity in near-surface zones [15, 19]. However, applicability of microelectrodes to measure local conductivities in LLZO has not been proven yet.

In this contribution it is shown that microelectrode impedance spectroscopy can be applied on LLZO. Comparison is made between the overall performance of an Al stabilized sample and local Li-ion conductivities, obtained by ionically blocking microelectrodes (Ø: 20–300 μm) [20–22]. A scattering of conductivities within one and the same sample was found. In addition, changes of the spectra measured by microelectrodes before and after long-time exposure to ambient air revealed the degradation of near-surface regions in such measurements.

2 Experimental

2.1 Sample preparation

Samples with a nominal composition of $Li_{6.40}Al_{0.20}La_3Zr_2O_{12}$ were investigated. The synthesis route is based on the procedure described by Wagner et al. [23]. Li_2CO_3 (99%, Merck), Al_2O_3 (99.5%, Aldrich), La_2O_3 (99.99%, Roth), and ZrO_2 (99.0%, Roth) were weighed to reach the intended stoichiometry with an excess of 10 wt% Li_2CO_3, with respect to the stoichiometric amount of Li_2CO_3. The reagents were ground and mixed in an agate mortar under addition of isopropyl alcohol and then pressed into pellets. The pellets were heated to 850 °C with a rate of 5 °C min^{-1} and calcinated for 4 h. After cooling down, the pellets were again ground in an agate mortar and ball-milled for 1 h under isopropyl alcohol (FRITSCH Pulverisette 7, 800 rpm, 2 mm ZrO_2 balls). After drying, the powder was pressed into pellets and put into an alumina crucible. To avoid undesired incorporation of Al^{3+} from the crucible and to suppress evaporation of Li_2O from the material, the sample pellets were placed between two additional pellets of pure $Li_7La_3Zr_2O_{12}$. The final sintering step was performed at 1230 °C for 6 h in ambient air. This results in a polycrystalline pellet with a diameter of about 7 mm, 4.6 mm thickness and typical LLZO-grain sizes of about 100–200 μm (Fig. 1). The density of the sample, measured by a pycnometer (Brand GmbH), is 91%.

2.2 Electrical measurement

The ionic conductivity was measured by electrochemical impedance spectroscopy (EIS). For measurements of the effective conductivity of macroscopic samples (macroelectrode measurements), samples were polished by grinding paper (#4000), and thin films of Pt (200 nm) and Ti (10 nm) were deposited on top and bottom as ionically blocking electrodes.

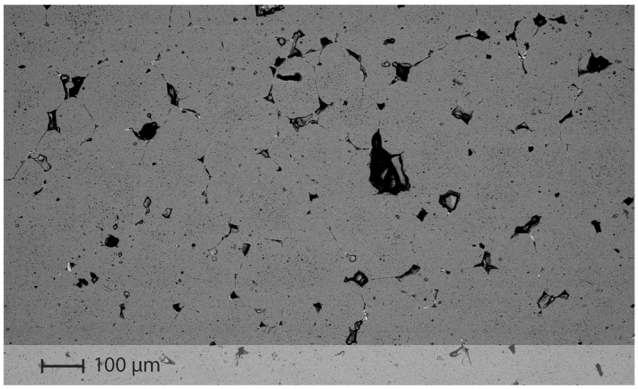

Fig. 1 SEM image of an aluminium stabilized LLZO (Al = 0.20) garnet after sintering at 1230 °C for 6 h. *Dark spots* indicate the existence of some pores

A thin film of titanium is required in order to improve the adhesion of platinum. For the EIS measurements, a Novocontrol Alpha Analyzer was used in the frequency range of 3×10^6–10 Hz. For such macroelectrode measurements the temperature was controlled by a Julabo F-25 HE thermostat, the exact temperature was 25.3 °C, determined by a thermocouple at the sample.

Local conductivities were measured by means of microelectrodes. Using photolithographic techniques in combination with ion beam etching, circular electrodes with diameters of 20–300 μm were prepared from the macroscopic Pt/Ti thin films on top of the samples. Microelectrode measurements were performed at ambient temperature (T = 23.5 °C). Tungsten needles were used to contact the microelectrodes under an optical microscope. The position of the needles was adjusted by mechanically controlled micromanipulators. Figure 2 (a) illustrates the measurement setup and (b) shows a part of the microelectrode array on top of the sample. Impedance measurements (Novocontrol Alpha Analyzer) were performed between a microelectrode and the counter electrode on the bottom side (Pt thin film with Pt paste at the sample edges for contact reasons).

3 Results and discussion

3.1 Macroelectrode measurements

Before microelectrodes were prepared from the Pt thin film the sample's overall performance was measured with the two macroscopic electrodes. The impedance spectrum of the Al stabilized LLZO garnet determined at 25.3 °C is plotted in Fig. 3. It shows a part of a "semicircle" at high frequencies, followed by a well separated low frequency contribution which represents the impedance of the ionically blocking electrodes (Ti/Pt). In agreement with earlier studies we attribute the resistance of the high frequency feature to ion conduction in the bulk [24, 25].

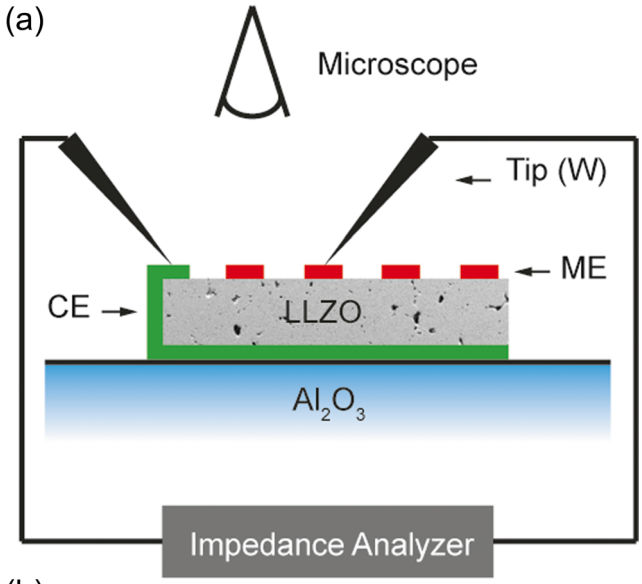

Fig. 2 (**a**) A scheme of the microelectrode measurement setup. (**b**) The optical microscope image shows a part of the microelectrode array on top of a sample

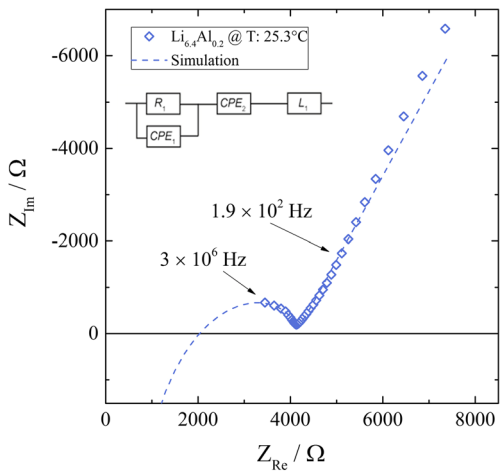

Fig. 3 The impedance spectra of an aluminium stabilized LLZO sample at 25.3 °C with measurement data (*diamonds*) and the simulation based on the fit to the equivalent circuit shown in the graph

In order to quantify the impedance spectrum properly, a resistor in parallel to a constant phase element ($R_1 \| CPE_1$) is used for the bulk contribution, in series to a constant phase element CPE_2 describing the blocking electrodes. Additionally, an inductive element (L) is required due to wiring; this is responsible for the strong distortion of the bulk semicircle and the real axis intercept at finite Z_{Re}, rather than at $Z_{Re} = 0$. Hence, the intercept at 2000 Ω in Fig. 3 is not an ohmic offset but the result of the serial inductance. The equivalent circuit shown in Fig. 3 leads to a reliable fit (dashed line) of the impedance spectrum and relative permittivities (ε_r) calculated from CPE_1 are in the range of 70, which confirms the bulk character of this part of the spectrum. The fit parameters of the spectrum in Fig. 3 are given in Table 1.

From the resistance R_1, the effective bulk conductivity σ_{macro} can be calculated by

$$\sigma_{macro} = \frac{h}{A\,R_1}\ \left[S\ cm^{-1}\right] \quad (1)$$

with h being the sample thickness and A the surface area. In this specific case a bulk conductivity of 3.3×10^{-4} S cm^{-1} results.

This is within the range typically found for such LLZO samples stabilized with aluminium [8, 13, 27–31]. However, literature data reveal a large scattering of bulk or total conductivities, and in a separate paper we will show that a substantial variation also exists between numerous nominally identical samples prepared in our labs. Compared to all data of our extensive study, the sample shown here has a rather good effective ionic bulk conductivity, even though also two times higher values were measured (A. Wachter-Welzl, et al. unpublished data).

3.2 Microelectrode measurements

While macroscopic electrodes only yield mean sample conductivities, microelectrodes provide the possibility to measure spatially resolved conductivities. Based on the principle that most of the voltage between a microelectrode and an extended counter electrode drops very close to the microelectrode, the diameter of the electrode (d) determines the investigated volume beneath. The measured resistances are largely determined by the conductivity of a hemisphere with a radius of $2d$ [16]. An array of microelectrodes with different diameters (20–300 μm) was measured at room temperature. Figure 4 displays typical impedance spectra found in such microelectrodes measurements on the LLZO sample.

Table 1 Calculated value of the ideal bulk capacity [26] and the relative permittivity

R_1 [Ω]	σ_{macro} [S cm^{-1}]	CPE_1[F s^{n-1}]	n_1	C_1 [F]	ε_r
4082	3.26×10^{-4}	1.19×10^{-11}	0.95	4.90×10^{-12}	74

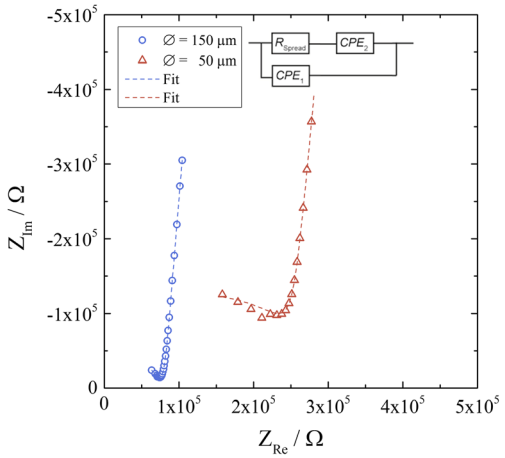

Fig. 4 Impedance spectra of two Ti/Pt microelectrodes with different diameter *d*, and the corresponding fits (*dashed line*) based on the equivalent circuit shown above

The high frequency arc corresponds to charge transport in the probed sample volume and is described by a resistive element (R_{Spread}) in the equivalent circuit. The low frequency capacitive increase is caused by the ionically blocking microelectrode and can be modelled by a constant phase element (*CPE2*), in agreement with the macroscopic electrodes. In many cases, the electrode response of microelectrodes was even steeper than for macroelectrodes and thus the exponent of the *CPE* closer to 1. Since macro- and microelectrodes consist of the same material, this suggests the existence of some regions with very non-ideal ion blocking, distributed across the sample. The latter probably cause the less steep electrode response in the macroelectrode measurements. In parallel to R_{Spread} and CPE_2, a stray capacitance (CPE_1) has to be introduced due to the measurement setup with a value in the range of 200 fF. This value is larger than what was expected for the bulk capacitance of most microelectrodes. Only for $d \geq 200$ µm a geometrical bulk capacitance ($C = 2\,\varepsilon_r\,\varepsilon_0\,d$, ε_0 = vacuum permittivity) in the 200 pF range results from $\varepsilon_r \approx 60$. However, adding the bulk capacitance to the equivalent circuit leads to an over parameterization and was therefore avoided here.

A fit of the impedance spectra to the equivalent circuit shown in Fig. 4 (dashed line) reveals R_{Spread} values. If this "spreading resistance" R_{Spread} is only due to the charge transport in the bulk, it can be used to calculate the local conductivity, see below. In principle, grain boundary resistances or other interfacial resistances with parallel capacitances being smaller than the stray capacitance cannot be separated from the high frequency arc and may thus also contribute to R_{Spread} [12]. Grain boundary related effects could not be observed in macroscopic impedance spectra and we do not expect an effect in the microelectrode measurements either. However, additional interfacial resistances cannot be excluded, cf. Sec. 3.3.

Figure 5 shows the resulting "spreading resistances" R_{Spread} of microelectrodes with a diameter of 100 µm (blue) and 200 µm (red). Variations are very moderate with standard

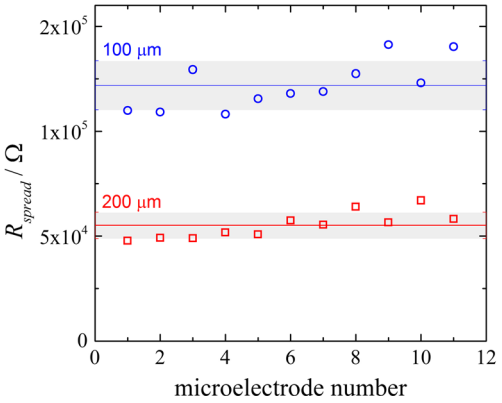

Fig. 5 Statistical distribution of the spreading resistance for 100 and 200 µm sized electrodes

deviations in the range of 9.5%. From the spreading resistance R_{Spread} and the microelectrode diameter *d*, a nominal bulk conductivity σ_{me} can be calculated [32] according to

$$\sigma_{me} = \frac{1}{2\,R_{spread}\,d}. \quad (2)$$

Provided the sample is homogeneous in the region beneath a microelectrode, this value reflects the true local Li-ion conductivity. Figure 6 displays nominal σ_{me} values for microelectrodes with different diameters. The solid line σ_{macro} represents the effective conductivity of the sample, measured with macroelectrodes before microelectrodes were prepared from the macroelectrode on top. Within a factor of about two, macroscopic and microscopic conductivities agree. This indicates that local conductivity measurements using microelectrodes are meaningful and that microelectrode measurements are indeed possible on LLZO. However, the ionic conductivity from microelectrodes seems to depend on their diameter. The averaged local conductivities found for 100 and 300 µm are 4.1×10^{-4} S cm^{-1} and 4.9×10^{-4} S cm^{-1} (Fig. 7), respectively and thus somewhat larger than the mean conductivity of the sample (3.3×10^{-4} S cm^{-1}). The highest value found for a

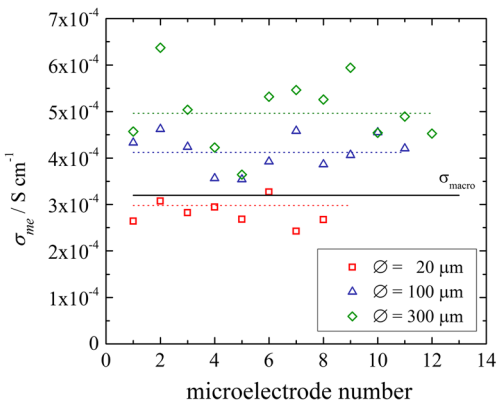

Fig. 6 Local conductivities found for differently sized microelectrodes compared to the overall effective performance of the sample (σ_{macro}). The *dotted lines* represent the mean values of the microelectrodes

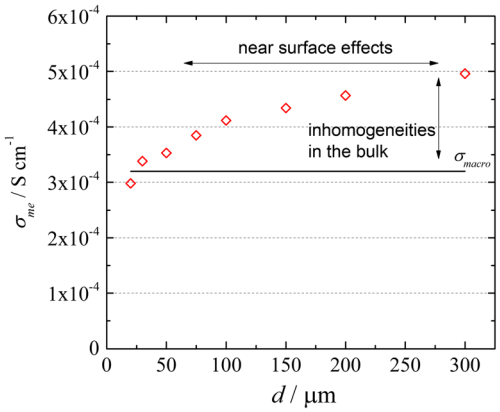

Fig. 7 The averaged local conductivities of differently sized microelectrodes. The conductivity increases with the diameter of the electrode

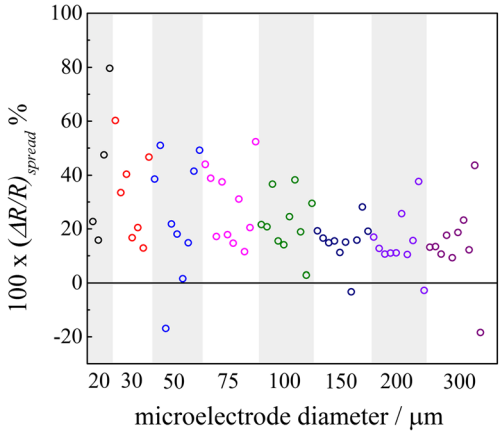

Fig. 9 The relative change in resistance R_{Spread} for differently sized electrodes measured after 3 weeks exposure to ambient air

300 µm microelectrode (6.3×10^{-4} S cm^{-1}) is even significantly higher than the values typically reported for LLZO stabilized with $Al_{0.20}$ (σ_{macro}: 2.4–3.4 × 10^{-4} S cm^{-1}) [7, 8, 31]. Plotting the averaged conductivity for every microelectrode diameter shows a clear trend (Fig. 7): For the smallest microelectrodes the measured conductivities are smallest and even slightly below σ_{macro}.

As small microelectrodes are most sensitive to near-surface effects, this suggests that near to the surface less conductive regions exist. Possibly, local stoichiometric deviations near to the surface or the formation of impurity phases or secondary phases (e.g. $La_2Zr_2O_7$, $LaAlO_3$, La_2O_3, $La(OH)_3$, Li_2CO_3, LiOH), are responsible for the lower nominal conductivities σ_{me} [14, 33–35], since preparation as well as measurements include exposure to air. Hou et al. investigated Al stabilized LLZO, sintered at 1100 °C, by means of laser induced breakdown spectroscopy (LIBS) as a surface sensitive measurement method [36]. The maximum depth reached in that contribution was about 35 µm, which is comparable to the range covered by microelectrodes with a diameter of 20 µm. LIBS measurements

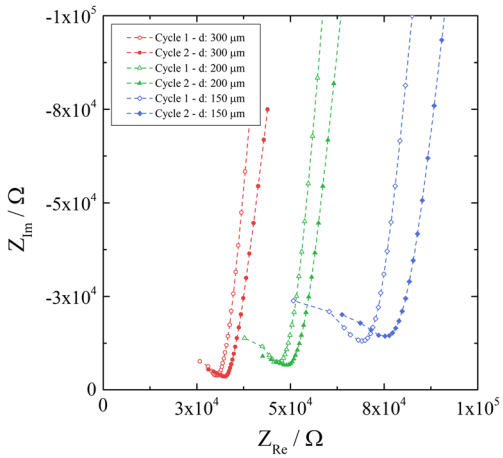

Fig. 8 Impedance spectra of different microelectrodes measured in the pristine state (cycle 1) and after three weeks exposed to ambient air (cycle 2). A change in the impedance spectra indicates conductivity degradation

detected aluminium and lithium rich phases in the first micrometres before the elemental distribution returns to a more or less equilibrated state. In addition, also misorientation angles may affect the ionic conductivity [35]. This could also contribute to the lower local conductivities found here.

The higher conductivity found for larger microelectrodes however, has to have a different reason. Most probably, the samples exhibit spatially inhomogeneous cation compositions and thus the effective conductivities from macroscopic measurements also include sample regions with smaller conductivity while the microelectrodes used in this study seem to be located on regions with higher conductivity. Indeed, in a related study on the scatter of effective sample conductivities of nominally identical samples we could identify significant conductivity variations not only from sample to sample but also within a given sample (A. Wachter-Welzl, et al. unpublished data).

3.3 Near-surface degradation

Owing to their near-surface sensitivity, microelectrodes can also be used to investigate degradation phenomena originating close to the surface. Here, the same microelectrodes were measured again after three weeks of storage in ambient air. The impedance spectra in Fig. 8 display three different microelectrodes in their pristine state (cycle 1 – open symbols) and after long-time exposure to air (cycle 2 – filled symbols). Independent of the electrode diameter all impedance spectra indicate an increase in the resistance R_{Spread} compared to the pristine state.

These changes are probably related to near-surface degradation effects such as the formation of LiOH and Li_2CO_3 caused by a reaction with moisture and CO_2 from ambient air and the exchange of Li^+ by H^+ [9–11, 14]. Figure 9 summarize the measurements and illustrates the resistive changes between the pristine and the degraded state in dependence of the microelectrode diameter. Microelectrodes with a diameter of 20–50 µm show the largest changes with a maximum of 80% resistance increase. With increasing diameter, the variations

become smaller. This supports the assumption of near-surface degradation, which becomes less important as the probed volume beneath the electrode increases, i.e. as microelectrode diameters increase. Possibly a similar near-surface degradation already before the very first microelectrode measurements was also responsible for the low conductivities found for 20 μm microelectrodes on pristine samples (see Sec. 3.2).

4 Conclusion

It was shown that microelectrodes (Ø: 20–300 μm) can be successfully applied to a polycrystalline LLZO garnet sample and allowed microelectrode impedance spectroscopy studies. Those resulted in local information on bulk ionic conductivities. A comparison between the effective conductivity of the overall sample and conductivities of local areas of the sample revealed differences. Locally, conductivities were up to twice the effective bulk conductivity with a maximum local value of 6.3×10^{-4} S cm^{-1}. Reasons behind these conductivity differences are most probably compositional variations in the sample. Moreover, smaller microelectrodes lead to smaller nominal conductivities which indicates that near to the surface less conductive regions exist. The sensitivity of microelectrodes towards near-surface resistive changes was also used to investigate how exposure to ambient air affects the properties of LLZO samples. A substantial degradation of the local conductivity was found, particularly for small microelectrodes.

Acknowledgements Open access funding provided by TU Wien (TUW). The authors gratefully acknowledge The Austrian Research Promotion Agency (FFG), SoLiK project, for financial support.

Author contributions The manuscript was written through contributions of all authors. All authors have given approval to the final version of the manuscript.

References

1. J. Awaka, N. Kijima, H. Hayakawa, J. Akimoto, J. Solid State Chem. **182**, 2046–2052 (2009)
2. J. Awaka, A. Takashima, H. Hayakawa, N. Kijima, Y. Idemoto and J. Akimoto, Electroceramics in Japan XIV, **485**, 99–102, (2011)
3. R. Murugan, V. Thangadurai, W. Weppner, WILEY-VCH Verlag **46**, 7778–7781 (2007)
4. E. J. Cussen, J. Mater. Chem. **20**, 5167–5173 (2010)
5. V. Thangadurai, S. Narayanan, D. Pinzaru, Chem. Soc. Rev. **43**, 4714–4727 (2014)
6. Y. Zhang, F. Chen, R. Tu, Q. Shen, L. Zhang, J. Power Sources **268**, 960–964 (2014)
7. M. Kotobuki, K. Kanamura, Y. Sato, T. Yoshida, J. Power Sources **196**, 7750–7754 (2011)
8. Y. Li, J.-T. Han, C.-A. Wang, S. C. Vogel, H. Xie, M. Xu, J. B. Goodenough, J. Power Sources **209**, 278–281 (2012)
9. Y. Jin, P. J. McGinn, J. Power Sources **239**, 326–331 (2013)
10. C. Ma, E. Rangasamy, C. Liang, J. Sakamoto, K. L. More, M. Chi, Angew. Chem. **127**, 131–135 (2015)
11. Z. F. Yow, Y. L. Oh, W. Gu, R. P. Rao, S. Adams, Solid State Ionics **292**, 122–129 (2016)
12. L. Cheng, E. J. Crumlin, W. Chen, R. Qiao, H. Hou, S. F. Lux, V. Zorba, R. Russo, R. Kostecki, Z. Liu, Phys. Chem. Chem. Phys. **16**, 18294–18300 (2014)
13. L. Cheng, J. S. Park, H. Hou, V. Zorba, G. Chen, T. Richardson, J. Cabana, R. Russo, M. Doeff, J. Mater, Chem. A **2**, 172–181 (2014)
14. A. Aguadero, F. Aguesse, C. Bernuy-López, W. W. Manalastas, J. M. L. del Amo and J. A. Kilner, (2015)
15. J. Fleig, J. Maier, Solid State Ionics **85**, 9–15 (1996)
16. J. Fleig, J. Maier, Phys. Chem. Chem. Phys. **1**, 3315–3320 (1999)
17. J.-S. Lee, J. Fleig, J. Maier, T.-J. Chung, D.-Y. Kim, Solid State Ionics **176**, 1711–1716 (2005)
18. D. Rettenwander, A. Welzl, S. Pristat, F. Tietz, S. Taibl, G. Redhammer, J. Fleig, J. Mater, Chem. A **4**, 1506–1513 (2016)
19. J. Fleig, Solid State Ionics **161**, 279–289 (2003)
20. H. Buschmann, J. Dölle, S. Berendts, A. Kuhn, P. Bottke, M. Wilkening, P. Heitjans, A. Senyshyn, H. Ehrenberg, A. Lotnyk, Phys. Chem. Chem. Phys. **13**, 19378–19392 (2011)
21. C. A. Geiger, E. Alekseev, B. Lazic, M. Fisch, T. Armbruster, R. Langner, M. Fechtelkord, N. Kim, T. Pettke, W. Weppner, Inorg. Chem. **50**, 1089–1097 (2010)
22. J. Wolfenstine, J. Sakamoto, J. Allen, J. Mater. Sci. **47**, 4428–4431 (2012)
23. R. Wagner, G. n. Redhammer, D. Rettenwander, A. Senyshyn, W. Schmidt, M. Wilkening, G. Amthauer, Chem. Mater. **28**, 1861–1871 (2016)
24. D. Rettenwander, A. Welzl, L. Cheng, J. Fleig, M. Musso, E. Suard, M. M. Doeff, G. J. Redhammer, G. Amthauer, Inorg. Chem. **54**, 10440–10449 (2015)
25. R. Wagner, G. J. Redhammer, G. Tippelt, A. Welzl, S. Taibl, J. Fleig, A. Franz, W. Lottermoser, G. Amthauer, Chem. Mater. accepted (2016). doi:10.1021/acs.chemmater.6b02516
26. J. Fleig, Solid State Ionics **150**, 181–193 (2002)
27. Y. Zhang, J. Cai, F. Chen, R. Tu, Q. Shen, X. Zhang, L. Zhang, J. Alloys Compd. **644**, 793–798 (2015)
28. Y. Matsuda, K. Sakamoto, M. Matsui, O. Yamamoto, Y. Takeda, N. Imanishi, Solid State Ionics **277**, 23–29 (2015)
29. W. E. Tenhaeff, E. Rangasamy, Y. Wang, A. P. Sokolov, J. Wolfenstine, J. Sakamoto, N. J. Dudney, ChemElectroChem **1**, 375–378 (2014)
30. E. Rangasamy, J. Wolfenstine, J. Sakamoto, Solid State Ionics **206**, 28–32 (2012)
31. C.-L. Tsai, E. Dashjav, E.-M. Hammer, M. Finsterbusch, F. Tietz, S. Uhlenbruck, H. P. Buchkremer, J. Electroceram. **35**, 25–32 (2015)
32. F. Llewellyn-Jones, Oxford University Press, **15**, (1957)
33. W. Xia, B. Xu, H. Duan, Y. Guo, H. Kang, H. Li, H. Liu, ACS Appl. Mater. Interfaces **8**, 5335–5342 (2016)
34. L. Cheng, C. H. Wu, A. Jarry, W. Chen, Y. Ye, J. Zhu, R. Kostecki, K. Persson, J. Guo, M. Salmeron, ACS Appl. Mater. Interfaces **7**, 17649–17655 (2015)
35. S. R. Catarelli, D. Lonsdale, L. Cheng, J. Syzdek and M. Doeff, *Frontiers in Energy Research*, **4**, (2016). doi:10.3389/fenrg.2016.00014
36. H. Hou, L. Cheng, T. Richardson, G. Chen, M. Doeff, R. Zheng, R. Russo, V. Zorba, J. Anal. At. Spectrom. **30**, 2295–2302 (2015)